

An efficient likelihood-free Bayesian inference method based on sequential neural posterior estimation

Yifei Xiong^{1,2}, Xiliang Yang³, Sanguo Zhang^{1,2}, Zhijian He^{3*}

¹School of Mathematical Sciences, University of Chinese Academy of Sciences, Beijing, China

²Key Laboratory of Big Data Mining and Knowledge Management, Chinese Academy of Sciences, Beijing, China

³School of Mathematics, South China University of Technology, Guangzhou, China

Abstract

Sequential neural posterior estimation (SNPE) techniques have been recently proposed for dealing with simulation-based models with intractable likelihoods. Unlike approximate Bayesian computation, SNPE techniques learn the posterior from sequential simulation using neural network-based conditional density estimators. This paper reclaims SNPE-B proposed by Lueckmann et al. (2017), which suffers from inefficiency and slow inference due to inefficient utilization of simulated data and high variance of parameter updates. To address these issues, we firstly introduce a concentrated loss function based on an adaptive calibration kernel that reweights the simulated data appropriately to improve the data efficiency. Moreover, we provide a theoretical analysis of the variance of associated Monte Carlo estimators. Based on this analysis, we then propose several variance reduction techniques to further accelerate the process of learning. Numerical experiments demonstrate that our method outperforms the original method together with other existing competitors on certain tasks.

1 Introduction

Simulator based models are extensively used in a vast number of applications in science, including neuroscience [38], physics [8, 19] biology [23, 9] and inverse graphics [44], since it is an important tool to describe and understand the process being investigated from the provided observation. When applying traditional Bayesian inference on simulator based model, one finds difficulties like intractable likelihood function $p(x|\theta)$ and running the simulator may be computationally expensive and so on.

*Corresponding author: hezhijian@scut.edu.cn

To address these challenges, a series of likelihood-free Bayesian computation (LFBC) methods have been developed. These methods aim to perform Bayesian inference without explicitly calculating the likelihood function, such as approximate Bayesian computation (ABC) [4, 35] and synthetic likelihoods (SL) [51, 43], Bayes optimization [22], likelihood-free inference by ratio estimation [47] and pseudo marginals methods [1, 2].

Currently, optimization-based approaches are widely employed for LFBC. These approaches aim to minimize the Kullback-Leibler (KL) divergence between the variational density $q_\phi(\theta)$ and the posterior distribution $p(\theta|x_o)$. One prominent optimization-based approach is the variational Bayes (VB) method. In the likelihood-free context, progress has been made in applying VB. Barthelmé and Chopin [3] utilized expectation propagation, a variational approximation algorithm, to approximate posteriors. He et al. [24] developed an unbiased VB method based on nested Multi-level Monte Carlo to handle intractable likelihoods. However, these approaches require nested simulations to estimate the gradient estimator, resulting in additional computational cost.

In recent research, there has been a growing interest in combining neural networks with classic VB methods, particularly using neural network architectures like normalizing flows [29]. The integration of neural networks and VB provides a flexible and powerful framework for density estimation, offering multiple choices for the variational density. This combination has gained attention due to its outstanding performance. Sequential neural likelihood (SNL) method [41] approximates the likelihood $p(x|\theta)$ by neural network-based density estimator $q_\phi(x|\theta)$, then evaluates posterior density based on it; sequential neural ratio estimation (SNRE) method [25, 15, 36] computes the approximation ratio of likelihood without evaluating the true likelihood; neural posterior estimation (NPE) method approximates the true posterior density $p(\theta|x)$ by a neural posterior estimator $q_{F(x,\phi)}(\theta)$, where $F(x, \phi)$ denotes a neural network structure. When the inference problem is performed only on observation x_o , data efficiency can be improved with sequential training schemes proposed in the sequential neural posterior estimation (SNPE) method [39, 32, 20]: model parameters are drawn from the proposal, a more informative distribution about x_o compared to prior distribution. Meanwhile, SNPE requires a modification of the loss function called ‘correction step’ compared to NPE to make sure $q_{F(x,\phi)}(\theta)$ is the approximation of the real posterior $p(\theta|x)$. Many approaches are developed to solve this problem. All of these methods are summarized and reviewed in [10] and they have all been benchmarked in [34].

Our work is based on the weighted SNPE method proposed by Lueckmann et al. [32], specifically known as SNPE-B, which may suffer from inefficiency and slow inference due to inefficient utilization of simulated data and high variance of parameter update. To overcome these two difficulties, we propose a type of concentrated loss function based on an adaptive calibration kernel that appropriately reweights the simulated data to improve data efficiency. A theoretical analysis of the variance of the Monte Carlo estimator is provided to guide the design of variance reduction techniques. Based on this analysis, several variance reduction techniques are proposed together with theoretical guarantees. Finally, a comprehensive comparative analysis of our proposed methods with some existing methods is carried out on numerical experiments.

The rest of this paper is organized as follows. In Section 2, we review the basic SNPE formulation together with the SNPE-B algorithm and illuminate their limitations. In Section 3, we firstly introduce calibration kernel technique and establish a theory to analyze its variance, with which we identify three issues that could lead to excessive variance of our method, including unstable density ratio, the trade off of the bandwidth of calibration kernel and limited training samples. For these three problems, we have proposed corresponding solutions for each of them, they are adaptive calibration kernel method, sample recycling strategy and defensive sampling. We also examine the mass leakage problem in this section and propose the corresponding solution. In Section 4, some numerical experiments are conducted to support the advantages of our proposed methods. Section 5 concludes the main features of our strategies and points out the possible directions of future work by summarizing some of the remaining problems of our strategies.

2 Background

Let $p(\theta)$ be the prior of the model parameter of interest, given an observed sample x_o of interest, we aim to make inference on the posterior distribution $p(\theta|x_o) \propto p(\theta)p(x_o|\theta)$. However, in most cases, the likelihood function $p(x|\theta)$ either does not have an explicit expression or is difficult to evaluate, but can be expressed in the form of a ‘simulator’, that is, given a fixed model parameter θ , we can generate samples $x \sim p(x|\theta)$.

Likelihood-free inference can be viewed as a problem of conditional density estimation. In such framework, a conditional density estimator $q_{F(x,\phi)}(\theta)$, such as neural network-based density estimator, where ϕ stands for the parameter of the density estimator, is used to approximate $p(\theta|x)$ [40, 13, 20]. When training $q_{F(x,\phi)}(\theta)$ When training the approximation $q_{F(x,\phi)}(\theta) \approx p(\theta|x)$, our objective is to minimize the average KL divergence under marginal $p(x)$, corresponding to

$$\begin{aligned} & \mathbb{E}_{p(x)} [\mathcal{D}_{\text{KL}}(p(\theta|x)||q_{F(x,\phi)}(\theta))] \\ &= \iint p(x)p(\theta|x) (\log p(\theta|x) - \log q_{F(x,\phi)}(\theta)) dx d\theta \\ &= -\mathbb{E}_{p(\theta,x)} [\log q_{F(x,\phi)}(\theta)] + \iint p(\theta,x) \log p(\theta|x) dx d\theta \\ &:= L(\phi) + \iint p(\theta,x) \log p(\theta|x) dx d\theta, \end{aligned} \tag{1}$$

where the KL divergence $\mathcal{D}_{\text{KL}}(p(\theta)||q(\theta)) = \int p(\theta) \log \frac{p(\theta)}{q(\theta)} d\theta$ and $p(x) = \int p(\theta)p(x|\theta)d\theta$. Since the second integral is unrelated to ϕ , minimizing the loss function $L(\phi)$ is equivalent to minimizing the expected KL divergence of $p(\theta|x)$ and $q_{F(x,\phi)}(\theta)$ with respect to $x \sim p(x)$. Since $L(\phi)$ is intractable, we train with its unbiased estimator instead, i.e.,

$$\hat{L}(\phi) = -\frac{1}{N} \sum_{i=1}^N \log q_{F(x_i,\phi)}(\theta_i),$$

where the training data $\{(\theta_i, x_i)\}_{i=1}^N$ are sampled from the joint probability density $p(\theta, x) = p(\theta)p(x|\theta)$. After training, $p(\theta|x_o)$ can be easily approximated by $q_{F(x_o, \phi)}(\theta)$.

Since the conditional density estimation at x_o is ultimately used, a distribution $\tilde{p}(\theta)$ which is more informative about x_o instead of $p(\theta)$ is preferred to generate θ , which is called proposal. After initializing $\tilde{p}(\theta)$ as $p(\theta)$, we then want the approximation of $p(\theta|x_o)$ to serve as a good proposal in the following simulation. This conditional density estimation with adaptively chosen proposal is called *sequential neural posterior estimation* (SNPE). However, by replacing the joint density $p(\theta, x)$ with $\tilde{p}(\theta, x) = p(x|\theta)\tilde{p}(\theta)$ in $L(\phi)$, it turns out that $q_{F(x_o, \phi)}(\theta)$ approximates the so-called *proposal posterior*, which is defined as

$$\tilde{p}(\theta|x) = p(\theta|x) \frac{\tilde{p}(\theta)p(x)}{p(\theta)\tilde{p}(x)}, \quad (2)$$

where $\tilde{p}(x) = \int \tilde{p}(\theta)p(x|\theta)d\theta$. Hence adjustment towards the loss function $L(\phi)$ is required. The mainstream approaches to addressing this problem can be mainly categorized into three methods: SNPE-A [39], SNPE-B [32], and APT (also known as SNPE-C) [20].

The SNPE-A method, as outlined by Papamakarios and Murray [39], constrains the distribution $q_{F(x, \phi)}(\theta)$ to a specific structure, such as a mixture of Gaussians (MoG). The prior distribution $p(\theta)$ and proposal distribution $\tilde{p}(\theta)$ are restricted to be selected only from the normal distribution and Gaussian distribution. This approach enables a closed-form solution post-training, given by

$$q'_{F(x, \phi)}(\theta) = q_{F(x, \phi)}(\theta) \frac{p(\theta)\tilde{p}(x)}{\tilde{p}(\theta)p(x)},$$

subsequently, an approximation of the posterior $p(\theta|x_o)$ is achieved through $q'_{F(x_o, \phi)}(\theta)$. However, a limitation arises when the covariance matrix of some components in $q'_{F(x_o, \phi)}(\theta)$ becomes non-positive definite. This occurs if the proposal $\tilde{p}(\theta)$ is narrower than some component of $q_{F(x_o, \phi)}(\theta)$, leading to potential failure of the method.

Greenberg et al. [20] proposed the Automatic Posterior Transformation (APT) method, formulated as follows. Let

$$\tilde{q}_{F(x, \phi)}(\theta) = q_{F(x, \phi)}(\theta) \frac{\tilde{p}(\theta)}{p(\theta)} \frac{1}{Z(x, \phi)},$$

where $Z(x, \phi) = \int q_{F(x, \phi)}(\theta)\tilde{p}(\theta)/p(\theta)d\theta$ represents a normalization constant. Following [39, Proposition 1], when $\tilde{q}_{F(x, \phi)}(\theta)$ converges to *proposal posterior* $\tilde{p}(\theta|x)$, it implies that $q_{F(x, \phi)}(\theta)$ converges to $p(\theta|x)$. To compute $Z(x, \phi)$, this paper propose the atomic method, which enables the analytical computation of $Z(x, \phi)$ by setting $\tilde{p}(\theta)$ as a discrete distribution. However, this method requires nested simulation when calculating $Z(x, \phi)$, which implies additional simulation and computational costs.

The SNPE-B method, introduced by Lueckmann et al. [32], avoid this issue by in-

corporating an additional density ratio into the loss function:

$$\begin{aligned}\mathbb{E}_{\tilde{p}(\theta,x)} \left[\frac{p(\theta)}{\tilde{p}(\theta)} \log q_{F(x,\phi)}(\theta) \right] &= \iint \tilde{p}(\theta)p(x|\theta) \frac{p(\theta)}{\tilde{p}(\theta)} \log q_{F(x,\phi)}(\theta) dx d\theta \\ &= \mathbb{E}_{p(\theta,x)} [\log q_{F(x,\phi)}(\theta)].\end{aligned}\tag{3}$$

Its unbiased estimator is then given as: $\hat{L}(\phi) = -\frac{1}{N} \sum_{i=1}^N \frac{p(\theta_i)}{\tilde{p}(\theta_i)} \log q_{F(x_i,\phi)}(\theta_i)$. Consequently, model parameters θ may be drawn from any proposal [41], and this proposal may even be chosen using active learning [22, 33, 27].

SNPE-B suffers from unstable training as it is demonstrated in Figure 3, one of the obvious and main reasons is due to the small density of $\tilde{p}(\theta)$ on denominator. What's more, it also suffers from low data efficiency. Although only the performance of the density estimator near x_o is of interest, the KL divergence in the loss of SNPE-B are minimized in the sense of the expectation of $p(x)$ as it is stated in Eq.(3). Given the limited sample size of x , this could lead to an inefficient approximation since KL divergence between density estimator and $p(\theta|x)$ is also minimized on other x that far from x_o , while $p(\theta|x_o)$ is of interest. To address these two issues, we propose a series of methods, including calibration kernel and defensive sampling.

3 Methods

3.1 Improving data efficiency: the Calibration kernels way

The Eq.(3) indicates the inefficient expected approximation of $p(\theta|x)$ by $q_{F(x,\phi)}(\theta)$. However, since only the posterior $p(\theta|x)$ at the specific observed sample x_o is of interest, it is desirable to minimized the KL divergence around x_o rather than over the entire distribution $p(x)$. One approach to accomplish this is to incorporate a kernel function $K_\tau(x, x_o)$ which is introduced by Blum and François [6], quantifying the proximity of the data point x to x_o , the point of interest. One popular choice is the Gaussian kernel function, which can be expressed as $K_\tau(x, x_o) = (2\pi)^{-d/2} \tau^{-d} \exp(-\|x - x_o\|_2^2 / (2\tau^2))$, where τ is known as *bandwidth* of the kernel function and d is the dimension of data x .

In order to account for the impact of variations in the magnitudes of different components of x on the distance $\|x - x_o\|_2^2$, the Mahalanobis distance can be employed [42, 16]. It is defined as $\|x - x_o\|_M^2 = (x - x_o)^\top \Sigma^{-1} (x - x_o)$, where Σ denotes the covariance matrix of x , it may be estimated using $\hat{\Sigma} = \frac{1}{N-1} \sum_{i=1}^N (x_i - \bar{x})(x_i - \bar{x})^\top$, where $\bar{x} = \frac{1}{N} \sum_{i=1}^N x_i$. The Mahalanobis distance is invariant to scaling compared with Euclidean distance. Using the Mahalanobis distance, the modified Gaussian kernel function is given by $K_\tau(x, x_o) = (2\pi)^{-d/2} |\Sigma|^{-1/2} \tau^{-d} \exp(-(x - x_o)^\top \Sigma^{-1} (x - x_o) / (2\tau^2))$, where τ is a positive parameter called the *calibration kernel rate*. We then arrive at a new

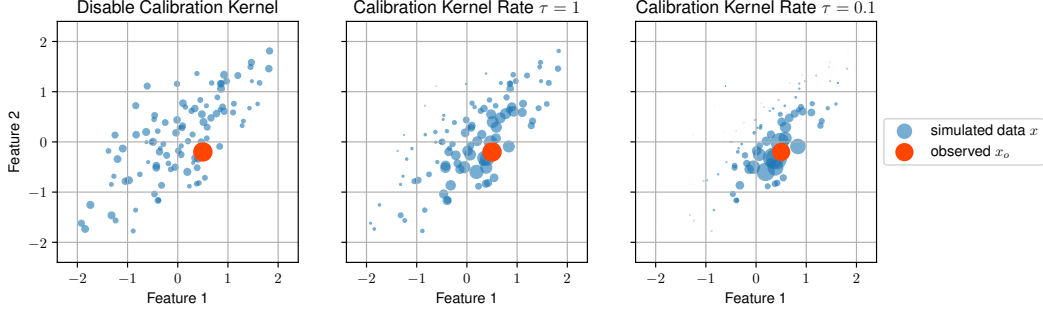


Figure 1: The calibration kernel adjusts the sample weights around x_o , where larger points are assigned higher weights. Left plot: only the density ratio $p(\theta)/\tilde{p}(\theta)$ is used to weight each sample, without considering the calibration kernel. Middle plot: the calibration kernel with rate $\tau = 1$ is incorporated to adjust the sample weights. Right plot: the calibration kernel is applied with rate $\tau = 0.1$.

weighted loss function Eq.(4) and its unbiased estimator Eq.(5)

$$\begin{aligned}
L_{\text{CK}}(\phi) &:= \mathbb{E}_{\tilde{p}(\theta, x)} \left[-K_\tau(x, x_o) \frac{p(\theta)}{\tilde{p}(\theta)} \log q_{F(x, \phi)}(\theta) \right] \\
&= \int p(x) K_\tau(x, x_o) \left[\int p(\theta|x) \log \left(\frac{p(\theta|x)}{q_{F(x, \phi)}(\theta)} \right) d\theta \right] dx + \text{Const} \\
&= C_\tau \mathbb{E}_{p_{\tau, x_o}(x)} [\mathcal{D}_{\text{KL}}(p(\theta|x) \| q_{F(x, \phi)}(\theta))] + \text{Const}, \tag{4}
\end{aligned}$$

$$\hat{L}_{\text{CK}}(\phi) = -\frac{1}{N} \sum_{i=1}^N K_\tau(x_i, x_o) \frac{p(\theta_i)}{\tilde{p}(\theta_i)} \log q_{F(x_i, \phi)}(\theta_i), \tag{5}$$

where $p_{\tau, x_o}(x) := p(x)K_\tau(x, x_o)/C_\tau$ and $C_\tau := \int p(x)K_\tau(x, x_o)dx$. It is worth mentioning that the density $p_{\tau, x_o}(x)$ will put more mass in the neighborhood of x_o , especially for small values of τ . Figure 1 illustrates the impact of the calibration kernel on sample weight when selecting different τ . This can be seen as a rare event sampling method, where rare events refer to the neighborhood of x_o in the sense of Mahalanobis or Euclidean distance.

Selecting different values for τ results in a trade-off between variance and efficiency. Calibration kernel can be thought of function that ‘assigns weight’ to any observation x according to its distance with x_o with scaling τ , so this weight itself can be seen as following a Gaussian distribution. When a rather small τ is given, the distribution becomes ‘peak’: it only assigns large weights to those x that close to x_o , resulting in an accurate approximation. The consequence comes with it is that most of the samples may have been ignored among the training due to their small weight being assigned, resulting in an unstable inference. In extreme situations where τ tends to 0, the encountered distribution degenerates to a Dirac function and the only observation available in training is x_o , indicating that in most cases there will be few or even no samples to use. When a moderate large τ is used, the distribution becomes flat, hence similar weights will be

assigned to all samples and therefore inefficient but stable inference. This insight is examined in greater detail in the following theorem.

Theorem 3.1. *Let*

$$\begin{aligned}\mu(\tau) &:= \mathbb{E}_{\tilde{p}(\theta,x)} [K_\tau(x, x_o) g(\theta, x)], \\ V(\tau) &:= \text{Var}_{\tilde{p}(\theta,x)} [K_\tau(x, x_o) g(\theta, x)], \\ h_g(x) &:= \int g(\theta, x) \tilde{p}(\theta, x) d\theta.\end{aligned}$$

Assume that $h_g(x)$ and $h_{g^2}(x)$ are twice continuously differentiable with bounded second-order derivatives. As $\tau \rightarrow 0$, we have

$$\mu(\tau) = h_g(x_o) + \mathcal{O}(\tau^2), \quad (6)$$

$$V(\tau) = Ch_{g^2}(x_o) \tau^{-d} + \mathcal{O}(\tau^{2-d}), \quad (7)$$

where $C = (2\pi)^{-d/2} 2^{-d/2} |\Sigma|^{-1/2}$.

The proof is detailed in Appendix A. As a result, the variance of the estimator $\text{Var}(\hat{L}_{\text{CK}}(\phi_t))$ and the variance of the gradient estimator $\text{Var}(\nabla_\phi \hat{L}_{\text{CK}}(\phi_t))$ are given respectively,

$$\text{Var}(\hat{L}_{\text{CK}}(\phi_t)) = V_1(\phi_t) \tau^{-d} N^{-1} + \mathcal{O}(\tau^{2-d} N^{-1}), \quad (8)$$

$$\text{Var}(\nabla_\phi \hat{L}_{\text{CK}}(\phi_t)) = V_2(\phi_t) \tau^{-d} N^{-1} + \mathcal{O}(\tau^{2-d} N^{-1}), \quad (9)$$

where

$$V_1(\phi) = Cp(x_o) \int \frac{p(\theta)}{\tilde{p}(\theta)} (\log q_{F(x_o, \phi)}(\theta))^2 p(\theta|x_o) d\theta, \quad (10)$$

and similarly,

$$V_2(\phi) = Cp(x_o) \int \frac{p(\theta)}{\tilde{p}(\theta)} (\nabla_\phi \log q_{F(x_o, \phi)}(\theta))^2 p(\theta|x_o) d\theta. \quad (11)$$

From Eq.(8) and Eq.(9), we conclude that these three main issues should be solved to improve the performance of the SNPE-B method after Calibration kernels technique is applied:

The first issue, as it is indicated by Eq.(10) and Eq.(11) that small-density areas of $\tilde{p}(\theta)$ can lead to excessive variance.

The second issue is the sample size N . While increasing N can be beneficial for variance reduction, the cost of performing multiple simulations can be prohibitively expensive. The sampling recycling technique [20] has been proven to be a useful method to address this issue. Due to the special formulation of importance sampling, further improvements can be made.

The last one is about the choice of τ . Eq.(6) indicates that a sufficiently small τ allows us to infer the true value of the posterior density at x_o . However, as $\tau \rightarrow 0$ in Eq.(7), $V(\tau) = \mathcal{O}(\tau^{-d})$ increases exponentially, leading to the curse of dimension. This poses a trade-off problem where we need to choose a proper τ to balance efficiency and variance.

3.2 Reducing variance in SNPE-B: our proposed method

3.2.1 Defensive sampling-based variance control

It is shown in the estimator in Eq.(3) that a relatively small value of the proposal $\tilde{p}(\theta)$ for $\theta_i \sim \tilde{p}(\theta)$ can result in an exceedingly large value of the density ratio $p(\theta_i)/\tilde{p}(\theta_i)$. This, in turn, can cause a substantial increase in the variance of the loss function as it is indicated in Eq.(8) and Eq.(9). It would be sufficient to address this issue by ensuring the heavy tail of the proposal $\tilde{p}(\theta)$ compared to the prior $p(\theta)$. As an essential problem in importance sampling community, defensive sampling, which is reported in [26, 37], has been proven to be a piratical solution. Pick α with $0 < \alpha < 1$ and choose

$$p_\alpha(\theta) = (1 - \alpha)q_{F(x_o, \phi)}(\theta) + \alpha p_{\text{def}}(\theta), \quad (12)$$

as the proposal distribution rather than $q_{F(x_o, \phi)}(\theta)$, where $p_{\text{def}}(\theta)$ is called the defensive density, with the ‘ideal property’ of being easily sampled and avoiding excessively low density, e.g. uniform distribution. Then an acceptable upper bound for $\frac{p(\theta)}{p_{\text{def}}(\theta)}$ is guaranteed, from Eq.(10), the variance of the estimator of the loss function $\text{Var}(\hat{L}(\phi_t))$ is well controlled by noticing

$$\int \frac{p(\theta)}{p_\alpha(\theta)} (\log q_{F(x_o, \phi)}(\theta))^2 p(\theta|x_o) d\theta \leq \frac{1}{\alpha} \int \frac{p(\theta)}{p_{\text{def}}(\theta)} (\log q_{F(x_o, \phi)}(\theta))^2 p(\theta|x_o) d\theta, \quad (13)$$

where the right hand side is bounded for $\frac{p(\theta)}{p_{\text{def}}(\theta)}$ is bounded, the variance of the gradient estimator Eq.(11) can be controlled in a similar way. This method is summarized as Algorithm 1.

Algorithm 1 SNPE-B method with calibration kernel and defensive sampling

- 1: Initialization: $\tilde{p}(\theta) := p(\theta)$, given $\alpha \in (0, 1)$, number of rounds R , simulations per round N
 - 2: **for** $r = 1, 2, \dots, R$ **do**
 - 3: sample $\{\theta_i\}_{i=1}^N$ from $\tilde{p}(\theta)$
 - 4: sample $x_i \sim p(x|\theta_i), i = 1, 2, \dots, N$, resulting in $\{x_i\}_{i=1}^N$
 - 5: update $\phi^* := \arg \min_{\phi} -\frac{1}{N} \sum_{i=1}^N \frac{p(\theta_i)}{\tilde{p}(\theta_i)} K_{\tau}(x_i, x_o) \log q_{F(x_i, \phi)}(\theta_i)$
 - 6: set $\tilde{p}(\theta) = (1 - \alpha)q_{F(x_o, \phi^*)}(\theta) + \alpha p_{\text{def}}(\theta)$
 - 7: **end for**
 - 8: **return** $q_{F(x_o, \phi^*)}(\theta)$
-

3.2.2 Multiple importance sampling and recycling

One effective way to , it can be beneficial to train $q_{F(x,\phi)}(\theta)$ on samples from previous rounds. Specifically, let N_r denote the number of parameter samples generated in the r th round, where the corresponding proposal is denoted as $\tilde{p}_r(\theta)$. The parameters sampled from the proposal in the r th round are denoted as $\theta_1^{(r)}, \dots, \theta_{N_r}^{(r)}$, along with the corresponding observations generated with the simulator $x_1^{(r)}, \dots, x_{N_r}^{(r)}$, where $r = 1, \dots, R$. Note that for any choice of proposal in rounds $k \leq r$, $-\frac{1}{N_k} \sum_{i=1}^{N_k} \frac{p(\theta_i^{(k)})}{\tilde{p}_k(\theta_i^{(k)})} K_\tau(x_i^{(k)}, x_o) \log q_{F(x_i^{(k)}, \phi)}(\theta_i^{(k)})$ is an unbiased estimator of $L_{\text{CK}}(\phi)$ given by Eq.(4). Therefore, aggregating the loss functions in the first r rounds may yield a better unbiased estimator of $L_{\text{CK}}(\phi)$, given by

$$L_1^{(r)}(\phi) = \sum_{k=1}^r \left(-\frac{1}{N_k} \sum_{i=1}^{N_k} \frac{p(\theta_i^{(k)})}{\tilde{p}_k(\theta_i^{(k)})} K_\tau(x_i^{(k)}, x_o) \log q_{F(x_i^{(k)}, \phi)}(\theta_i^{(k)}) \right). \quad (14)$$

On the other hand, inspired by the multiple importance sampling method [49], we can construct a better estimator of the corresponding form

$$L_\omega^{(r)}(\phi) = \sum_{k=1}^r \left(-\frac{1}{N_k} \sum_{i=1}^{N_k} \omega_k(\theta_i^{(k)}) \frac{p(\theta_i^{(k)})}{\tilde{p}_k(\theta_i^{(k)})} K_\tau(x_i^{(k)}, x_o) \log q_{F(x_i^{(k)}, \phi)}(\theta_i^{(k)}) \right). \quad (15)$$

Here $\omega_k(\cdot)$ can be considered as a non-negative weight function and $\{\omega_k(\cdot)\}_{k=1}^r$ is a partition of unity, satisfying $\sum_{k=1}^r \omega_k(\theta) = 1$ for all θ . One way of selecting weights with nearly optimal variance is to take $\omega_k(\theta) \propto N_k \tilde{p}_k(\theta)$, which is also known as balance heuristic strategy. In this case, the balance heuristic strategy is highly effective as confirmed by the following theorem. We denote this unbiased estimator of loss based on the balance heuristic strategy as L_{BH} , which has the following form

$$L_{\text{BH}}^{(r)}(\phi) = \sum_{k=1}^r \left(-\frac{1}{N_k} \sum_{i=1}^{N_k} \omega_k^{\text{BH}}(\theta_i^{(k)}) \frac{p(\theta_i^{(k)})}{\tilde{p}_k(\theta_i^{(k)})} K_\tau(x_i^{(k)}, x_o) \log q_{F(x_i^{(k)}, \phi)}(\theta_i^{(k)}) \right), \quad (16)$$

where $\omega_k^{\text{BH}}(\theta) = \frac{N_k \tilde{p}_k(\theta)}{\sum_{k=1}^r N_k \tilde{p}_k(\theta)}$.

Theorem 3.2. *Let $L_\omega^{(r)}(\phi)$ and $L_{\omega_{\text{BH}}}^{(r)}(\phi)$ be the loss estimators given in Eq.(15) and Eq.(16), respectively. Then*

$$\text{Var} \left(L_{\omega_{\text{BH}}}^{(r)}(\phi) \right) \leq \text{Var} \left(L_\omega^{(r)}(\phi) \right) + \left(\frac{1}{\min_k N_k} - \frac{1}{\sum_{k=1}^r N_k} \right) L_{\text{CK}}(\phi)^2,$$

where $L_{\text{CK}}(\phi)$ is given by Eq.(4).

Proof. This is an application of [49, Theorem 1]. □

This method is referred as multiple importance sampling and recycling (MISR).

3.2.3 Adaptive calibration kernel based on ESS Criterion

This section presents an adaptive selection method for determining appropriate τ values in training process. Recall that in Eq.(6), as $\tau \rightarrow 0$,

$$L(\phi) = p(x_o)\mathcal{D}_{\text{KL}}(p(\theta|x_o)||q_{F(x_o,\phi)}(\theta)) + \text{Const} + \mathcal{O}(\tau^2).$$

As a result, when τ is small enough,

$$\underset{\phi}{\operatorname{argmin}} L(\phi) \approx \underset{\phi}{\operatorname{argmin}} \mathcal{D}_{\text{KL}}(p(\theta|x_o)||q_{F(x_o,\phi)}(\theta)),$$

indicating that we should choose τ as small as possible. However, small τ will lead to a large variance of estimator due to Eq.(8).

In our basic setting, for a minibatch of samples, the weight and size of these samples serve as two indicator of their importance for training. It comes with the insight that the larger the weight and sample size of a minibatch of samples, the greater their importance in training. When selecting τ , two types of samples may be obtained. If τ is large, the obtained samples will be a batch of samples with similar weights. If τ is small, the obtained samples will consist of a small portion of samples larger weights and a large portion of samples with smaller weights. It may be difficult to compare the effects of these two types of the samples for both indicators vary.

Effective sampling size (ESS) proposed in Del Moral et al. [12], by incorporating sample weight and the sample size, it indicates ‘the real size of samples in training’, which is defined as

$$\text{ESS} = \frac{\left(\sum_{i=1}^N w_i\right)^2}{\sum_{i=1}^N w_i^2},$$

where $w_i = \frac{p(\theta_i)}{\bar{p}(\theta_i)}K_\tau(x_i, x_o)$ in Algorithm 1.

In the absence of MISR, the number of samples used in each round remains constant. A common criterion for ESS selection in this scenario is to define it as a fraction of the current iteration’s sample size N , i.e., $\text{ESS} = \beta N$. For analytical ease, we introduce the concept of the *effective ratio*, representing the ratio of ESS to the number of samples utilized in each round. In each round, after simulating the set $\{(\theta_i, x_i)\}_{i=1}^N$, the value of τ is numerically determined by solving the equation $\text{ESS} = \beta N$ using the bisection method. This approach achieves a balance between the bias and variance of the estimator.

The introduction of MISR significantly alters the sampling framework. Here, the count of samples per round equates to the cumulative number of generated samples, denoted as rN . As training rounds increase, the total number of generated samples tends towards infinity. This change required a modification of the ESS selection, particularly due to that *effective ratio* decreases to $\frac{1}{rN}$ as τ approaches zero. To accommodate the increasing rounds and expanding sample pool under MISR, it is essential to adaptively modulate the *effective ratio*. The goal is to progressively focus the model on more pertinent samples, specifically those proximal to x_o .

In response, we propose a refined ESS selection method: $\text{ESS} = f(r)\beta N$, where the *effective ratio* is now becomes $\frac{f(r)\beta}{r}$. One approach is to maintain a constant $f(r)$, such

Table 1: Comparison of different $f(r)$ (measured with C2ST¹)

Task	M/G/1	Lotka-Volterra	SLCP	g-and-k
$f_1(r)$	0.658 (0.625, 0.682)	0.934 (0.908, 0.943)	0.875 (0.817, 0.925)	0.724 (0.677, 0.749)
$f_2(r)$	0.638 (0.618, 0.654)	0.925 (0.915, 0.939)	0.824 (0.798, 0.847)	0.708 (0.687, 0.737)

as $f_1(r) = 1$, resulting in a constant ESS. Another strategy aims for $f(r)$ to grow with each round but still satisfy the condition that $\frac{f(r)}{r}$ tends towards 0. In this case, we consider $f_2(r) = \log(r - 1 + e)$, which aligns the ESS with the standard approach in the initial round. Table 1 simulates the numerical results of these two selection methods across four tasks, indicating superior outcomes for the latter in numerical simulations. Detailed information about the tasks and metrics is elaborated in Section 4.

3.3 Solving mass leakage: Parameter space transformation

In some cases, the support of the prior of model parameter, $\text{supp}(p(\theta)) = \{\theta \in \mathbb{R}^n | p(\theta) > 0\}$, is a bounded area, where $n = \dim(\theta)$, but $q_{F(x,\phi)}(\theta)$ usually represents a density whose support is unbounded, as does $\hat{p}(\theta)$. When a sample pair (θ, x) falls outside the $\text{supp}(p(\theta))$, its weight will be assigned as 0, effectively rejecting the sample. However, this can result in wasted samples and data inefficiency, particularly when running the simulator is expensive. Moreover, the mismatched support sets can also lead to mass leakage.

One feasible solution to this problem is truncation [20], which estimates the normalization factor after training $q_{F(x,\phi)}(\theta)$. However, this method can also lead to a significant amount of mass being leaked outside the prior support. Another efficient method is to sample only from the truncated proposal [11], which requires an additional computational step to reject samples and may still result in mass leakage. These approaches may generate samples from the proposal that lie outside $\text{supp}(p)$ and require additional post-processing steps.

One way to essentially solve mass leakage is to remap the parameter space. Suppose there exists a reversible transformation $h(\cdot)$ such that the density function of $\hat{\theta} := h(\theta)$ is \hat{p} and satisfies $\text{supp}(\hat{p}) = \{x \in \mathbb{R}^n | \hat{p}(x) > 0\} = \mathbb{R}^n$. If $h(\cdot)$ is strictly monotone and invertible on each dimension of $\text{supp}(p)$, then $\hat{\theta}$ has density

$$\hat{p}(\theta) = p(h^{-1}(\theta)) \left| \frac{\partial}{\partial \theta} h^{-1}(\theta) \right|,$$

Using this transformation, it is possible to train $q_{F(x,\phi)}(\theta)$ on an unbounded support space derived from the transformed input. Additionally, once the posterior density $\hat{p}(\hat{\theta}|x_o)$ has been obtained in the transformed space, we can transform it back to the original parameter space using:

$$p(\theta|x_o) = \hat{p}(h(\theta)|x_o) \left| \frac{\partial}{\partial \theta} h(\theta) \right|.$$

This trick requires an invertible monotonic mapping $h(\cdot)$. Although it simple case like a bounded high-dimensional rectangle $[a_1, b_1] \times \cdots \times [a_n, b_n] \subset \mathbb{R}^n$, we can take $h(\theta) = \left(\ln\left(\frac{\theta_1 - a_1}{b_1 - \theta_1}\right), \dots, \ln\left(\frac{\theta_n - a_n}{b_n - \theta_n}\right) \right)^\top$ that transformed $\text{supp}(p)$ to \mathbb{R}^n . In more complex cases, invertible monotonic mapping $h(\cdot)$ could be difficult to construct due to complex forms of $\text{supp}(p)$. In this case, h can be constructed on a rough region $K \subset \mathbb{R}^n$ such that $\text{supp}(p) \subset K$, and continues to combined with the truncation method [20, 11]. This prevents the density from leaking in regions $\mathbb{R}^n \setminus K$. If the difference between K and $\text{supp}(p)$ is small, it can further prevent a large amount of mass being leaked outside.

The transformation of parameter space is sometimes necessary since drawing samples from posterior distribution that lies inside the supporting set of prior is costing in certain circumstances as it is reported in [18].

4 Experiments

In this section, we conduct a series of comparative analysis of our proposed strategies with existing methods to demonstrate their effectiveness. Since our strategies is built upon the SNPE-B method, hence we begin with an ablation study. Subsequently, we then compare our methods with other likelihood-free Bayesian computation methods such as SNPE-A [39], APT [20] and SNL [41].

It is notable that our strategies has no restrictions on the type of $q_{F(x,\phi)}(\theta)$. To minimize the impact of its structure on numerical results, we employ neural spline flows (NSFs) [14] as the conditional density estimators, which is highly flexible and has been widely applied in related research as evidenced by [34, 11]. Our NSFs consists of 8 layers. Each layer is constructed using two residual blocks with 50 units and ReLU activation function. With 10 bins in each monotonic piecewise rational-quadratic transform, and the tail bound is set to 20.

We illustrate only parts of the experiments and their result in this section, the rest of the experiments and their result are supplemented in Appendix C .

M/G/1 model [45]. The model describes a single server’s processing of a queue of continuously arriving jobs. Define I as the total number of jobs that needs to be processed, and denote by s_i the processing time required for job i . Let v_i be the job’s arrival time in the queue, and d_i be the job’s departure time from the queue. They satisfy the following conditions

$$\begin{aligned} s_i &\sim \mathcal{U}(\theta_1, \theta_1 + \theta_2), \\ v_i - v_{i-1} &\sim \text{Exp}(\theta_3), \\ d_i - d_{i-1} &= s_i + \max(0, v_i - d_{i-1}). \end{aligned}$$

In our experiments, we configured $I = 50$, and selected the summary statistics $S(x)$ to be the logarithms of 0th, 25th, 50th, 75th and 100th percentiles of the set of inter-departure times. The prior distribution of the parameters is

$$\theta_1 \sim \mathcal{U}(0, 10), \theta_2 \sim \mathcal{U}(0, 10), \theta_3 \sim \mathcal{U}(0, 1/3),$$

and our experiments choose ground truth parameter as

$$\theta^* = (1, 4, 0.2).$$

The observed summary statistic $S(x_o)$ simulated from the model with ground truth parameter θ^* is

$$S(x_o) = (0.0929, 0.8333, 1.4484, 1.9773, 3.1510),$$

and the corresponding standard deviation under ground truth parameter θ^* (based on 10,000 simulations) is

$$s = (0.1049, 0.1336, 0.1006, 0.1893, 0.2918).$$

Lotka-Volterra model [50]. This model represents a Markov jump process that characterizes the dynamics of a predator population interacting with a prey population, with four parameters denoted as $\theta = (\theta_1, \dots, \theta_4)$. Let X be the number of predators, and Y be the number of prey. The model posits that the following events can occur:

- the birth of a predator at a rate $\exp(\theta_1)XY$, resulting in an increase of X by one.
- the death of a predator at a rate proportional to $\exp(\theta_2)X$, leading to a decrease of X by one.
- the birth of a prey at a rate proportional to $\exp(\theta_3)Y$, resulting in an increase of Y by one.
- the consumption of a prey by a predator at a rate proportional to $\exp(\theta_4)XY$, leading to a decrease of Y by one.

Following the experimental details in [41], we initialized the predator and prey populations as $X = 50$ and $Y = 100$ respectively. We performed simulations of the Lotka-Volterra model using the Gillespie algorithm [17] over a duration of 30 time units, and recorded the populations at intervals of 0.2 time units, resulting in two timeseries of 151 values each. The resulting summary statistics $S(x)$ is a 9-dimensional vector that comprises the following timeseries features: the log mean of each timeseries; the log variance of each timeseries; the autocorrelation coefficient of each timeseries at lags 0.2 and 0.4 time units; the cross-correlation coefficient between the two timeseries.

In our experiments, the prior distribution of the parameters is set to $\mathcal{U}(-5, 2)^4$, the ground truth parameters are

$$\theta^* = (\log 0.01, \log 0.5, \log 1, \log 0.01),$$

the observed summary statistics $S(x_o)$ simulated from the model with ground truth parameters θ^* are

$$S(x_o) = (4.6431, 4.0170, 7.1992, 6.6024, 0.9765, 0.9237, 0.9712, 0.9078, 0.0476),$$

and the corresponding standard deviation under ground truth parameters θ^* (based on 10,000 simulations) are

$$s = (0.3294, 0.5483, 0.6285, 0.9639, 0.0091, 0.0222, 0.0107, 0.0224, 0.1823).$$

To evaluate the degree of similarity between the approximate posterior distribution $q_{F(x_o, \phi)}(\theta)$ and the true posterior distribution $p(\theta|x_o)$ given the observed data, we utilize maximum mean discrepancy (MMD) [21] and classifier two sample tests (C2ST) [30] as a discriminant criterion. Another criterion for measurement is the log median distance (LMD) between x_o and x drawn from $p(x|\theta)$, where θ is sampled from $q_{F(x_o, \phi)}(\theta)$. In scenarios where the true posterior distribution $p(\theta|x_o)$ is intractable even with knowledge of the sample generation process, we employ the negative log probability (NLOG) of the true parameters θ^* , in this case, the observation x_o is sampled from $p(x|\theta^*)$. All the above four indicators are the lower the better.

Our numerical experiments were conducted on a computer equipped with a single GeForce RTX 2080s GPU and an i9-9900K CPU. The training and inference processes of the model were primarily implemented using the Pytorch package in Python.

In the training process, we simulate $N = 1000$ samples in each round, and there are a total of $R = 20$ rounds. In each round, we randomly pick 5% of the newly generated samples θ and their corresponding x values as validation data. We follow the early stop criterion proposed by Papamakarios et al. [41], which terminates the training if the loss value on the validation data does not decrease after 20 epochs in a single round. For the stochastic gradient descent optimizer, we use Adam [28] with a batch size of 100, a learning rate of 1×10^{-4} , and a weight decay of 1×10^{-4} .

4.1 Compare to original SNPE-B method

In this section we provide a detailed comparison of the performance of our proposed strategies, including adaptive calibration kernels (ACK), defensive sampling (DS), and multiple importance sampling and recycling (MISR) methods with the crude SNPE-B method. Recall that in the case of bounded supporting set of prior and so does the posterior while the supporting set of the neural posterior is unbounded, two types of strategies are considered in this paper in order to approximate the true posterior. The first one is known as truncated posterior (TP), in which we directly truncate the neural posterior after training, this method suffers from low sampling efficiency and leakage of mass. The second one is parameter space transformation (PST), which is proposed in Section 3.3.

To study the difference between PST and TP, we additionally examined these two cases with all other strategies in our experiment, which is represented as All (TP) and All (PST).

We evaluate the performance of our proposed strategies on four likelihood-free Bayesian problems: SLCP [41], Lotka-Volterra [31], g-and-k [24] and M/G/1 [45] model. When computing the log median distance between simulated and observed data, we normalize the calculation using standard deviation of each component of the samples

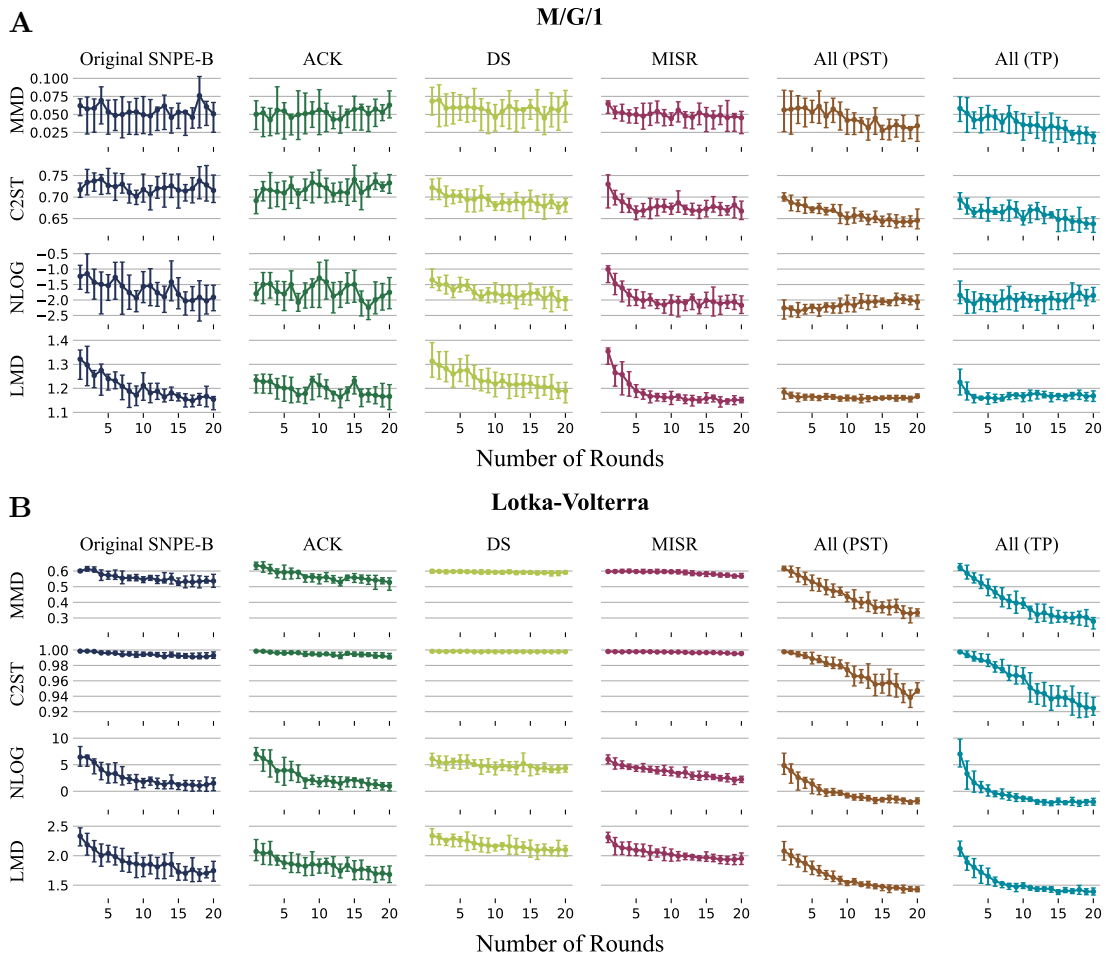


Figure 2: **Ablation experiments on proposed strategies.** **A.** Performance on M/G/1 queuing model. **B.** Performance on Lotka-Volterra predation model. The horizontal axis represents the round of training and the error bars represent the mean with the upper and lower quartiles. Our proposed methods exhibits better performance compared to the original method.

generated from the ground truth parameters. This was necessary because the samples produced by different models exhibited varying scales across dimensions. As an ablation experiment, Figure 2 illustrates the performance of each strategy, showing the following:

The ACK method results in a stable and accurate inference. Calibration kernel strategy, as it is illustrated in Eq.(4), yields a more accurate inference by replacing $p(x)$ with $p_{\tau, x_o}(x)$ in the loss function, making the training concentrate around x_o , improving the quality of samples especially in earlier training phases and leads to a more stable inference. However, with an increase in the number of training iterations, the advantage of ACK diminishes. This may be due to the fact that each round produces θ from

$q_{F(x_o, \phi)}(\theta)$ rather than a prior distribution $p(\theta)$ that is completely independent of x_o . This, to some extent, makes the performance of the model in the later training phases similar to that of the adaptive calibration kernels method, even without its incorporation.

The DS method stabilize training, as it is demonstrated in Figure 2, manifested as smaller error bar. By controlling the variance of the loss function and its gradient, this approach prevents undesirable simulation results from entering the training set. It performs particularly well under the negative log posterior density. What’s more, DS also help with mode collapse issues, since it defensive distribution enables the density estimator to still have the opportunity to explore the correct direction even when the learning of posterior is incorrect, which is likely to happen in the case of multimodal like SLCP. From the ablation experiment in Figure 2, we can see that the performance of the method has been greatly improved after using DS.

Compared with TP, the introduction of PST causes a transformation of the target. After incorporating this strategy, no significant negative impact on the performance was observed. However, it can be ensured that there is no mass leakage problem, and therefore, there is no need for additional calculations of the normalization constant when the posterior density is required at a given location, which can be computational expensive. Moreover, the efficiency of sampling can be greatly improved. In conclusion, one should always apply PST instead of TP when using our method. Its improvement towards APT is reported in [11].

MISR demonstrates excellent performance by increasing the number of training rounds because all the samples generated in the previous rounds are being reused. This is the most significant improvement among all of the aforementioned strategies.

After combining these strategies, our proposed method exhibits a significant improvement in performance compared to the original one. We also evaluate the performance of our proposed method in g-and-k model [24] and SLCP model [41], the detailed results are provided in Figure 5 (see Appendix D), where our proposed strategies works as well. In the case of SLCP, we observe that DS greatly solve the issue of ‘mode collapse’ encountered with the original SNPE-B, where metrics like MMD and C2ST increase with rounds because SNPE-B may ‘lose sight of some modes’ during training, and this can not be corrected since no more samples around the ‘lost modes’ will be generated. From which we concludes that the use of DS not only allows for a more thorough exploration of the parameter space, but also ensures the possibility of ‘returning to the right track again’ when situation like mode collapse arises.

We also report the result of the ablation study on SLCP and g-and-k model in Appendix D.

4.2 Compare to other likelihood-free inference methods

As it is demonstrated in Figure 3, our proposed improved SNPE-B methods achieve consistent and sometimes more accurate and faster inference compared with other methods, especially with APT on most of the tasks. What’s more, our proposed method reduces computational costs (total iteration step times the number of sample used in each iteration) by nearly 8 times compared to APT as it is demonstrated in Table 2. Although

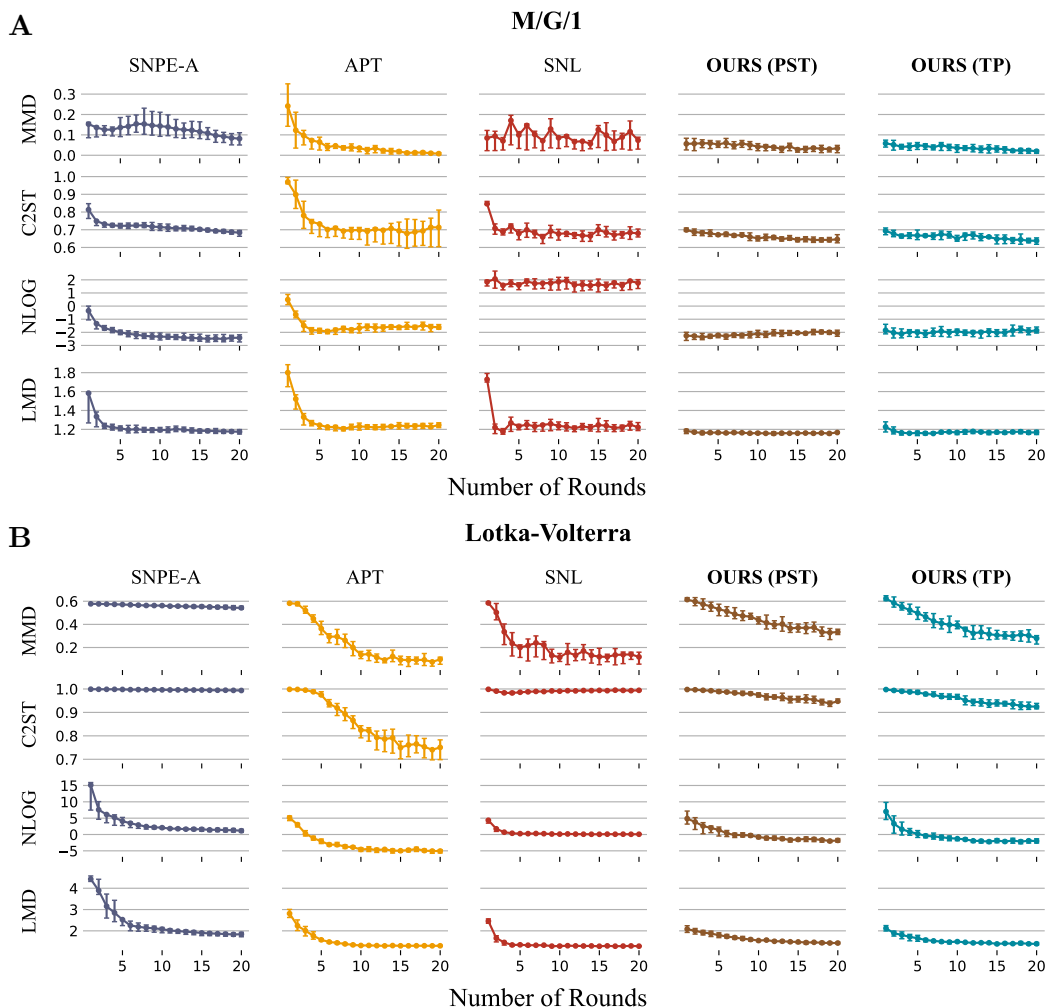


Figure 3: **Our proposed strategy versus other methods.** **A.** Performance on M/G/1 queuing model. **B.** Performance on Lotka-Volterra predation model. The horizontal axis represents the round of training and the error bars represent the mean with the upper and lower quartiles.

with the aid of several variance reduction techniques, the stability of our inference is still sometimes not good enough in early training stage. For example, in Lotka-Volterra model, the large variance of the second component of the observation leads to an unstable estimation of the covariance matrix in the calibration kernel when Mahalanobis distance is involved, probably causing an unstable inference in early training phases. Hence, a more robust estimation method is required. Visualizations of these approximated posterior is also provided in Figure 7 (see Appendix D).

Figure 4 illustrates the outcomes of the SMC-ABC method applied to the two models under same performance metrics. The results indicate that, after 20 iterations or 2×10^4

Table 2: Comparison of computational costs¹

Task	M/G/1	Lotka-Volterra	SLCP	g-and-k
APT	8.19 (7.75, 8.51)	8.22 (7.56, 8.78)	7.61 (7.21, 7.94)	8.01 (7.66, 8.45)
SNPE-B	1.19 (1.13, 1.25)	1.14 (1.03, 1.24)	0.87 (0.75, 0.99)	1.41 (1.13, 1.45)
OURS (PST)	1.07 (1.03, 1.11)	0.98 (0.94, 1.01)	0.81 (0.77, 0.84)	1.05 (0.99, 1.10)
OURS (TP)	1.18 (1.12, 1.23)	1.03 (0.97, 1.98)	0.75 (0.70, 0.78)	-

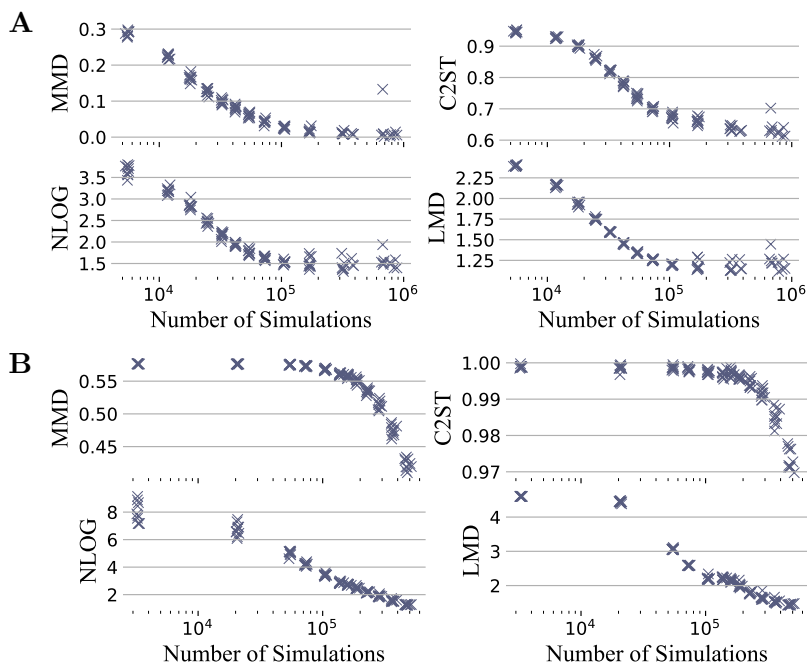


Figure 4: **Approximation accuracy by SMC-ABC method against number of simulations.** **A.** Performance on M/G/1 queuing model. **B.** Performance on Lotka-Volterra predation model.

simulations, our method achieved outcomes that are comparable to, or better than, those obtained by the SMC-ABC method after approximately 5×10^5 simulations.

5 Discussion

Techniques in Importance Sampling. Our work was inspired by several variance reduction techniques proposed in importance sampling methods, such as defensive sampling and multiple importance sampling. In contrast to the SNPE-A and APT methods, the performance of the original SNPE-B method may sometimes be suboptimal due to the additional density ratio attached to its loss function, resulting in larger variance of the loss function and its gradient during the training process. Based on these perspectives, we propose several methods and then be able to achieve a performance that is

consistent and sometimes better compared to original SNPE-B and APT by combining them.

Lower computational cost. Our method has an additional advantage of less computational training speed during the iteration step inherited from the SNPE-B method. Although the loss function we propose in Eq.(16) seems to be more complex than that of the original SNPE-B method, the ratio of densities and the value of the calibration kernel can be calculated after simulating new samples in each round of training, without the necessity to recalculate them during the multiple sub-iterations of that round. In fact, in each iteration, we only need to compute the value of $\log q_{F(x_i, \phi)}(\theta_i)$ for every sample pair (θ_i, x_i) in the minibatch, then multiply them by the pre-calculated coefficients. In contrast, the APT with atomic proposals method requires the computation of $\log q_{F(x_j, \phi)}(\theta_i)$ for all possible sample pairs (θ_i, x_j) in the minibatch, resulting in a computational complexity of $\mathcal{O}(M \times m)$, where M denotes the size of minibatch and m denotes the number of atoms in the algorithm proposed by APT. As a result, the computational efficiency of the APT method is inferior to that of the original SNPE-B method and our improved SNPE-B method, both of which have computational complexities of $\mathcal{O}(M)$. We also provide experimental results in Table 2.

Versatility. Since most of the NPE method can be finally broke down to the minimization of the KL divergence, the strategies we have proposed are transferable to other methods. For instance, the ACK strategy could be extended to the APT method and SNRE method, which may improve performance in the early rounds. The PST strategy can also be applied to the APT method to avoid the issue of density leakage. Unlike the SNPE-B method, ABC requires all θ to be within the support of the prior distribution. Introducing the PST method can avoid additional steps related to truncation through rejection sampling and estimating the normalization factor.

Acknowledgments

The work of the first author and third author was supported by the National Natural Science Foundation of China No.12171454, U19B2940 and Fundamental Research Funds for the Central Universities. The work of the fourth author was supported by the National Natural Science Foundation of China grant 12071154, the Guangdong Basic and Applied Basic Research Foundation grant 2021A1515010275.

References

- [1] C. Andrieu and G. O. Roberts. The pseudo-marginal approach for efficient Monte Carlo computations. *The Annals of Statistics*, 37(2):697 – 725, 2009.
- [2] C. Andrieu, A. Doucet, and R. Holenstein. Particle markov chain monte carlo methods. *Journal of the Royal Statistical Society: Series B (Statistical Methodology)*, 72(3):269–342, 2010.

- [3] S. Barthelmé and N. Chopin. Expectation propagation for likelihood-free inference. *Journal of the American Statistical Association*, 109(505):315–333, 2014.
- [4] M. A. Beaumont, W. Zhang, and D. J. Balding. Approximate Bayesian computation in population genetics. *Genetics*, 162(4):2025–2035, 2002.
- [5] M. A. Beaumont, J.-M. Cornuet, J.-M. Marin, and C. P. Robert. Adaptive approximate Bayesian computation. *Biometrika*, 96(4):983–990, 2009.
- [6] M. G. Blum and O. François. Non-linear regression models for Approximate Bayesian Computation. *Statistics and computing*, 20:63–73, 2010.
- [7] F. V. Bonassi and M. West. Sequential Monte Carlo with adaptive weights for approximate Bayesian computation. *Bayesian Analysis*, 10(1):171 – 187, 2015.
- [8] J. Brehmer, G. Louppe, J. Pavez, and K. Cranmer. Mining gold from implicit models to improve likelihood-free inference. *Proceedings of the National Academy of Sciences*, 117(10):5242–5249, 2020.
- [9] R. Clarke, H. W. Resson, A. Wang, J. Xuan, M. C. Liu, E. A. Gehan, and Y. Wang. The properties of high-dimensional data spaces: implications for exploring gene and protein expression data. *Nature reviews cancer*, 8(1):37–49, 2008.
- [10] K. Cranmer, J. Brehmer, and G. Louppe. The frontier of simulation-based inference. *Proceedings of the National Academy of Sciences*, 117(48):30055–30062, 2020.
- [11] M. Deistler, P. J. Goncalves, and J. H. Macke. Truncated proposals for scalable and hassle-free simulation-based inference. *arXiv preprint arXiv:2210.04815*, 2022.
- [12] P. Del Moral, A. Doucet, and A. Jasra. An adaptive sequential Monte Carlo method for approximate Bayesian computation. *Statistics and computing*, 22:1009–1020, 2012.
- [13] L. Dinh, J. Sohl-Dickstein, and S. Bengio. Density estimation using real nvp. *arXiv preprint arXiv:1605.08803*, 2016.
- [14] C. Durkan, A. Bekasov, I. Murray, and G. Papamakarios. Neural spline flows. *Advances in neural information processing systems*, 32, 2019.
- [15] C. Durkan, I. Murray, and G. Papamakarios. On contrastive learning for likelihood-free inference. In *International conference on machine learning*, pages 2771–2781. PMLR, 2020.
- [16] R. Erhardt and S. A. Sisson. Modelling extremes using approximate Bayesian computation. *Extreme Value Modelling and Risk Analysis*, pages 281–306, 2016.
- [17] D. T. Gillespie. Exact stochastic simulation of coupled chemical reactions. *The Journal of Physical Chemistry*, 81(25):2340–2361, 1977.

- [18] M. Glöckler, M. Deistler, and J. H. Macke. Variational methods for simulation-based inference. *arXiv preprint arXiv:2203.04176*, 2022.
- [19] P. J. Gonçalves, J.-M. Lueckmann, M. Deistler, M. Nonnenmacher, K. Öcal, G. Bassetto, C. Chintaluri, W. F. Podlaski, S. A. Haddad, T. P. Vogels, et al. Training deep neural density estimators to identify mechanistic models of neural dynamics. *Elife*, 9:e56261, 2020.
- [20] D. Greenberg, M. Nonnenmacher, and J. Macke. Automatic posterior transformation for likelihood-free inference. In *International Conference on Machine Learning*, pages 2404–2414. PMLR, 2019.
- [21] A. Gretton, K. M. Borgwardt, M. J. Rasch, B. Schölkopf, and A. Smola. A kernel two-sample test. *The Journal of Machine Learning Research*, 13(1):723–773, 2012.
- [22] M. U. Gutmann and J. Corander. Bayesian optimization for likelihood-free inference of simulator-based statistical models. *Journal of Machine Learning Research*, 2016.
- [23] M. Hashemi, A. N. Vattikonda, J. Jha, V. Sip, M. M. Woodman, F. Bartolomei, and V. K. Jirsa. Amortized Bayesian inference on generative dynamical network models of epilepsy using deep neural density estimators. *Neural Networks*, 163:178–194, 2023.
- [24] Z. He, Z. Xu, and X. Wang. Unbiased MLMC-based variational Bayes for likelihood-free inference. *SIAM Journal on Scientific Computing*, 44(4):A1884–A1910, 2022.
- [25] J. Hermans, V. Begy, and G. Louppe. Likelihood-free mcmc with amortized approximate ratio estimators. In *International conference on machine learning*, pages 4239–4248. PMLR, 2020.
- [26] T. Hesterberg. Weighted average importance sampling and defensive mixture distributions. *Technometrics*, 37(2):185–194, 1995.
- [27] M. Järvenpää, M. U. Gutmann, A. Pleska, A. Vehtari, and P. Marttinen. Efficient acquisition rules for model-based approximate Bayesian computation. *Bayesian Analysis*, 14(2):595 – 622, 2019.
- [28] D. P. Kingma and J. Ba. Adam: A method for stochastic optimization. *arXiv preprint arXiv:1412.6980*, 2014.
- [29] I. Kobyzev, S. J. Prince, and M. A. Brubaker. Normalizing flows: An introduction and review of current methods. *IEEE transactions on pattern analysis and machine intelligence*, 43(11):3964–3979, 2020.
- [30] D. Lopez-Paz and M. Oquab. Revisiting classifier two-sample tests. *arXiv preprint arXiv:1610.06545*, 2016.
- [31] A. J. Lotka. Analytical note on certain rhythmic relations in organic systems. *Proceedings of the National Academy of Sciences*, 6(7):410–415, 1920.

- [32] J.-M. Lueckmann, P. J. Goncalves, G. Bassetto, K. Öcal, M. Nonnenmacher, and J. H. Macke. Flexible statistical inference for mechanistic models of neural dynamics. *Advances in neural information processing systems*, 30, 2017.
- [33] J.-M. Lueckmann, G. Bassetto, T. Karaletsos, and J. H. Macke. Likelihood-free inference with emulator networks. In *Symposium on Advances in Approximate Bayesian Inference*, pages 32–53. PMLR, 2019.
- [34] J.-M. Lueckmann, J. Boelts, D. Greenberg, P. Goncalves, and J. Macke. Benchmarking simulation-based inference. In *International Conference on Artificial Intelligence and Statistics*, pages 343–351. PMLR, 2021.
- [35] J.-M. Marin, P. Pudlo, C. P. Robert, and R. J. Ryder. Approximate Bayesian computational methods. *Statistics and computing*, 22(6):1167–1180, 2012.
- [36] B. K. Miller, C. Weniger, and P. Forré. Contrastive Neural Ratio Estimation. *arXiv preprint arXiv:2210.06170*, 2022.
- [37] A. Owen and Y. Zhou. Safe and effective importance sampling. *Journal of the American Statistical Association*, 95(449):135–143, 2000.
- [38] L. Paninski and J. P. Cunningham. Neural data science: accelerating the experiment-analysis-theory cycle in large-scale neuroscience. *Current opinion in neurobiology*, 50:232–241, 2018.
- [39] G. Papamakarios and I. Murray. Fast ε -free inference of simulation models with bayesian conditional density estimation. *Advances in neural information processing systems*, 29, 2016.
- [40] G. Papamakarios, T. Pavlakou, and I. Murray. Masked autoregressive flow for density estimation. *Advances in neural information processing systems*, 30, 2017.
- [41] G. Papamakarios, D. Sterratt, and I. Murray. Sequential neural likelihood: Fast likelihood-free inference with autoregressive flows. In *The 22nd International Conference on Artificial Intelligence and Statistics*, pages 837–848. PMLR, 2019.
- [42] G. W. Peters, Y. Fan, and S. A. Sisson. On sequential Monte Carlo, partial rejection control and approximate Bayesian computation. *Statistics and Computing*, 22:1209–1222, 2012.
- [43] L. F. Price, C. C. Drovandi, A. Lee, and D. J. Nott. Bayesian synthetic likelihood. *Journal of Computational and Graphical Statistics*, 27(1):1–11, 2018.
- [44] L. Romaszko, C. K. Williams, P. Moreno, and P. Kohli. Vision-as-inverse-graphics: Obtaining a rich 3d explanation of a scene from a single image. In *Proceedings of the IEEE International Conference on Computer Vision Workshops*, pages 851–859, 2017.

- [45] A. Y. Shestopaloff and R. M. Neal. On Bayesian inference for the M/G/1 queue with efficient MCMC sampling. *arXiv preprint arXiv:1401.5548*, 2014.
- [46] S. A. Sisson, Y. Fan, and M. M. Tanaka. Sequential monte carlo without likelihoods. *Proceedings of the National Academy of Sciences*, 104(6):1760–1765, 2007.
- [47] O. Thomas, R. Dutta, J. Corander, S. Kaski, and M. U. Gutmann. Likelihood-free inference by ratio estimation. *Bayesian Analysis*, 17(1):1–31, 2022.
- [48] T. Toni, D. Welch, N. Strelkowa, A. Ipsen, and M. P. Stumpf. Approximate Bayesian computation scheme for parameter inference and model selection in dynamical systems. *Journal of the Royal Society Interface*, 6(31):187–202, 2009.
- [49] E. Veach and L. J. Guibas. Optimally combining sampling techniques for Monte Carlo rendering. In *Proceedings of the 22nd annual conference on Computer graphics and interactive techniques*, pages 419–428, 1995.
- [50] D. J. Wilkinson. *Stochastic Modelling for Systems Biology*. CRC press, 2018.
- [51] S. N. Wood. Statistical inference for noisy nonlinear ecological dynamic systems. *Nature*, 466(7310):1102–1104, 2010.

Appendix

A Proofs of Theorem 3.1

Proof. The effect of τ can be deduced from the following equations

$$\begin{aligned}
\mu(\tau) &= \mathbb{E}_{\tilde{p}(\theta, x)} [K_\tau(x, x_o) g(\theta, x)] \\
&= \int K_\tau(x, x_o) \left(\int g(\theta, x) \tilde{p}(\theta, x) d\theta \right) dx \\
&= \int K_\tau(x, x_o) h_g(x) dx \\
&= \int (2\pi)^{-d/2} |\Sigma|^{-1/2} \tau^{-d} \exp\left(-\frac{(x - x_o)^\top \Sigma^{-1} (x - x_o)}{2\tau^2}\right) h_g(x) dx \\
&= \int (2\pi)^{-d/2} |\Sigma|^{-1/2} \exp\left(-\frac{x^\top \Sigma^{-1} x}{2}\right) h_g(x_o + \tau x) dx \\
&= \int (2\pi)^{-d/2} |\Sigma|^{-1/2} \exp\left(-\frac{x^\top \Sigma^{-1} x}{2}\right) \left(h_g(x_o) + \tau x^\top \nabla_x h_g(x_o) + \mathcal{O}(\tau^2) \right) dx \\
&= h_g(x_o) + \mathcal{O}(\tau^2),
\end{aligned}$$

where $h_g(x) := \int g(\theta, x) \tilde{p}(\theta, x) d\theta$. On the other hand,

$$\begin{aligned}
V(\tau) &= \text{Var}_{\tilde{p}(\theta, x)} [K_\tau(x, x_o) g(\theta, x)] \\
&= \mathbb{E}_{\tilde{p}(\theta, x)} [K_\tau^2(x, x_o) g^2(\theta, x)] - (\mathbb{E}_{\tilde{p}(\theta, x)} [K_\tau(x, x_o) g(\theta, x)])^2 \\
&= \int K_\tau^2(x, x_o) h_{g^2}(x) dx - (h_g(x_o) + \mathcal{O}(\tau^2))^2 \\
&= \int (2\pi)^{-d} |\Sigma|^{-1} \tau^{-2d} \exp\left(-\frac{(x - x_o)^\top \Sigma^{-1} (x - x_o)}{\tau^2}\right) h_{g^2}(x) dx - (h_g(x_o) + \mathcal{O}(\tau^2))^2 \\
&= (2\pi)^{-d/2} 2^{-d/2} |\Sigma|^{-1/2} \tau^{-d} \int (2\pi)^{-d/2} |\Sigma|^{-1/2} \exp\left(-\frac{x^\top \Sigma^{-1} x}{2}\right) \\
&\quad \left(h_{g^2}(x_o) + \sqrt{2} \tau x^\top \nabla_x h_{g^2}(x_o) + \mathcal{O}(\tau^2)\right) dx - (h_g(x_o) + \mathcal{O}(\tau^2))^2 \\
&= (2\pi)^{-d/2} 2^{-d/2} |\Sigma|^{-1/2} \tau^{-d} h_{g^2}(x_o) + \mathcal{O}(\tau^{2-d}) - (h_g(x_o) + \mathcal{O}(\tau^2))^2 \\
&= C h_{g^2}(x_o) \tau^{-d} + \mathcal{O}(\tau^{2-d}),
\end{aligned}$$

where $C = (2\pi)^{-d/2} 2^{-d/2} |\Sigma|^{-1/2}$. □

B Summary statistics-based dimensional reduction

Using summary statistics enables us to reduce the dimension of the data being processed, by calculating relevant features, which in turn limits the impact of high-dimensional features that may be noisy or irrelevant. By doing so, we can mitigate the adverse effects of the curse of dimension and achieve more efficient and effective computations. The kernel function that incorporate the summary statistics is then

$$K_\tau^S(x, x_o) = (2\pi)^{-d_S/2} \tau^{-d_S} \exp\left(-\frac{(S(x) - S_o)^\top \Sigma_S^{-1} (S(x) - S_o)}{2\tau^2}\right),$$

where $d_S = \dim(S) \ll d = \dim(x)$ and Σ_S is estimated by $\hat{\Sigma}_S = \frac{1}{N-1} \sum_{i=1}^N (S(x_i) - \bar{S})(S(x_i) - \bar{S})^\top$, $\bar{S} = \frac{1}{N} \sum_{i=1}^N S(x_i)$ and $S_o = S(x_o)$. If the summary statistics are used, we also can use $p(\theta|S_o)$ to present $p(\theta|x_o)$, and both are equivalent when $S = S(x)$ is sufficient for θ . The corresponding algorithm is given in Algorithm 2.

C Additional model information

This section provide detailed information for SLCP and g-and-k model.

SLCP model [41]. The model has a complex and multimodal posterior form. Model parameters $\theta = (\theta_1, \dots, \theta_5)$ obeying a uniform prior on a bounded rectangle as $\mathcal{U}(-3, 3)^5$. The dimension of data x is 8, satisfying $p(x|\theta) = \prod_{i=1}^4 \mathcal{N}(x_{(2i-1, 2i)} | \mu(\theta), \Sigma(\theta))$, which is a two-dimensional normal distribution of four samples concatenated. The mean is defined by $\mu(\theta) = (\theta_1, \theta_2)^\top$ and the covariance matrix takes the form

$$\Sigma(\theta) = \begin{pmatrix} s_1^2 & \rho s_1 s_2 \\ \rho s_1 s_2 & s_2^2 \end{pmatrix},$$

Algorithm 2 Summary statistics-based dimensional reduction method

- 1: Initialization: $\tilde{p}(\theta) := p(\theta)$, given $\alpha \in (0, 1)$, number of rounds R , simulations per round N , given summary statistics $S(x)$, setting $S_o = S(x_o)$
 - 2: **for** $r = 1, 2, \dots, R$ **do**
 - 3: sample $\{\theta_i\}_{i=1}^N$ from $\tilde{p}(\theta)$
 - 4: sample $x_i \sim p(x|\theta_i), i = 1, 2, \dots, N$, resulting in $\{x_i\}_{i=1}^N$
 - 5: update $\phi^* = \arg \min_{\phi} -\frac{1}{N} \sum_{i=1}^N \frac{p(\theta_i)}{\tilde{p}(\theta_i)} K_{\tau}^S(x_i, x_o) \log q_{F(S(x_i), \phi)}(\theta_i)$
 - 6: set $\tilde{p}(\theta) := (1 - \alpha)q_{F(S(x_o), \phi^*)}(\theta) + \alpha p_{\text{def}}(\theta)$
 - 7: **end for**
 - 8: **return** $q_{F(x_o, \phi^*)}(\theta)$
-

where $s_1 = \theta_3^2$, $s_2 = \theta_4^2$ and $\rho = \tanh(\theta_5)$. In our experiments, the ground truth parameters are

$$\theta^* = (0.7, -2.9, -1, -0.9, 0.6),$$

and the observed data x_o simulated from the model with ground truth parameters θ^* are

$$x_o = (1.4097, -1.8396, 0.8758, -4.4767, -0.1753, -3.1562, -0.6638, -2.7063).$$

The standard deviation of each component of the data x generated from ground truth parameters θ^* are

$$s = (1, 0.81, 1, 0.81, 1, 0.81, 1, 0.81),$$

g-and-k model [24]. The univariate g-and-k distribution is a versatile, unimodal probability distribution that is capable of effectively characterizing data exhibiting substantial skewness and kurtosis. Its density function lacks a closed form representation, but can be alternatively expressed through its quantile function as

$$Q(q|\theta) = A + B \left[1 + 0.8 \frac{1 - \exp\{-gz(q)\}}{1 + \exp\{-gz(q)\}} \right] (1 + z(q)^2)^k z(q),$$

where $\theta = (A, B, g, k)$, $B > 0$, $k > -1/2$, and $z(q) = \Phi^{-1}(q)$ denotes the inverse CDF of $\mathcal{N}(0, 1)$. When both g and k are set to zero, it simplifies to a normal distribution. We adopt an unconstrained parameter vector denoted as $\tilde{\theta} = (A, \log B, g, \log(k + 1/2))$, corresponding prior distribution for $\tilde{\theta}$ is chosen as $\mathcal{N}(0, 4 \cdot I_4)$. The summary statistics we take are $S(x) = (S_A, S_B, S_g, S_k)$, where

$$\begin{aligned} S_A &= E_4, \\ S_B &= E_6 - E_2, \\ S_g &= (E_6 + E_2 - 2E_4)/S_B, \\ S_k &= (E_7 - E_5 + E_3 - E_1)/S_B, \end{aligned}$$

and $E_1 \leq \dots \leq E_7$ represent the empirical octiles of x . The ground truth parameters chosen for our experiments are

$$\theta^* = (3, 1, 2, 0.5),$$

the observed summary statistics $S(x_o)$ simulated from the model with ground truth parameters θ^* are

$$S(x_o) = (2.9679, 1.5339, 0.4691, 1.7889),$$

and the corresponding standard deviation under ground truth parameters θ^* (based on 10,000 simulations) are

$$s = (0.0395, 0.1129, 0.0384, 0.1219).$$

D Additional experimental results

This section provide experimental results including ablation experiments and comparative experiments with other SNPE method on SLCP and g-and-k model. We also provide visualisation of posterior estimated with our proposed method on four tasks.

We firstly report the result of ablation study of the proposed trick with Figure 5. Then, we report the result of comparative experiment with other SNPE method with Figure 6.

Figure 7 displays the posterior distribution estimates obtained by our method and other approaches. To obtain an approximate ground truth posterior for comparison purposes, we used the traditional SMC-ABC algorithm [5, 46, 7, 48] to estimate the posterior distribution. Our method outperforms the original SNPE-B method and exhibits similar performance to the APT method.

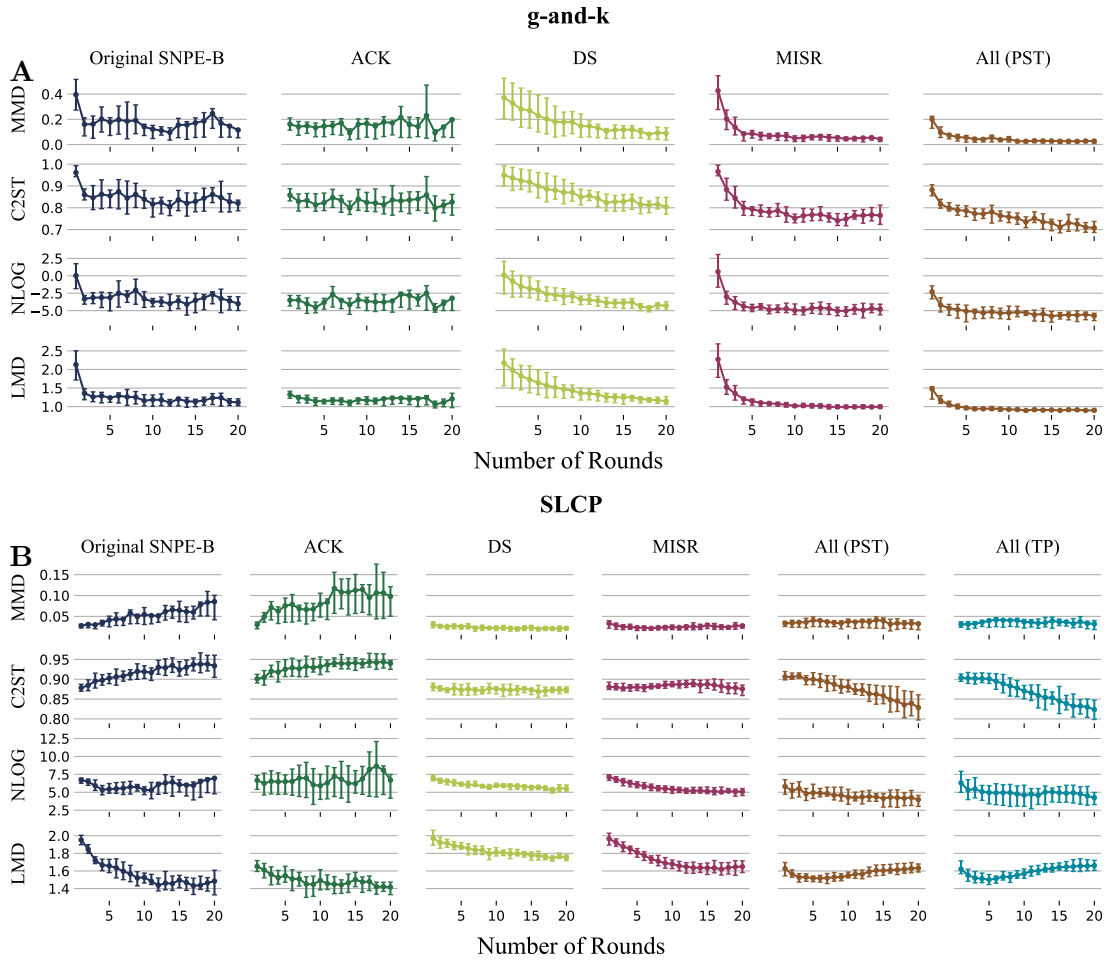


Figure 5: **Ablation experiments on proposed strategies.** Due to the unbounded prior for the g-and-k model, we can directly apply the neural posterior and we put the result of this problem in the column of All (PST). **A.** Performance on g-and-k model. **B.** Performance on SLCP model. The horizontal axis represents the round of training and the error bars represent the mean with the upper and lower quartiles.

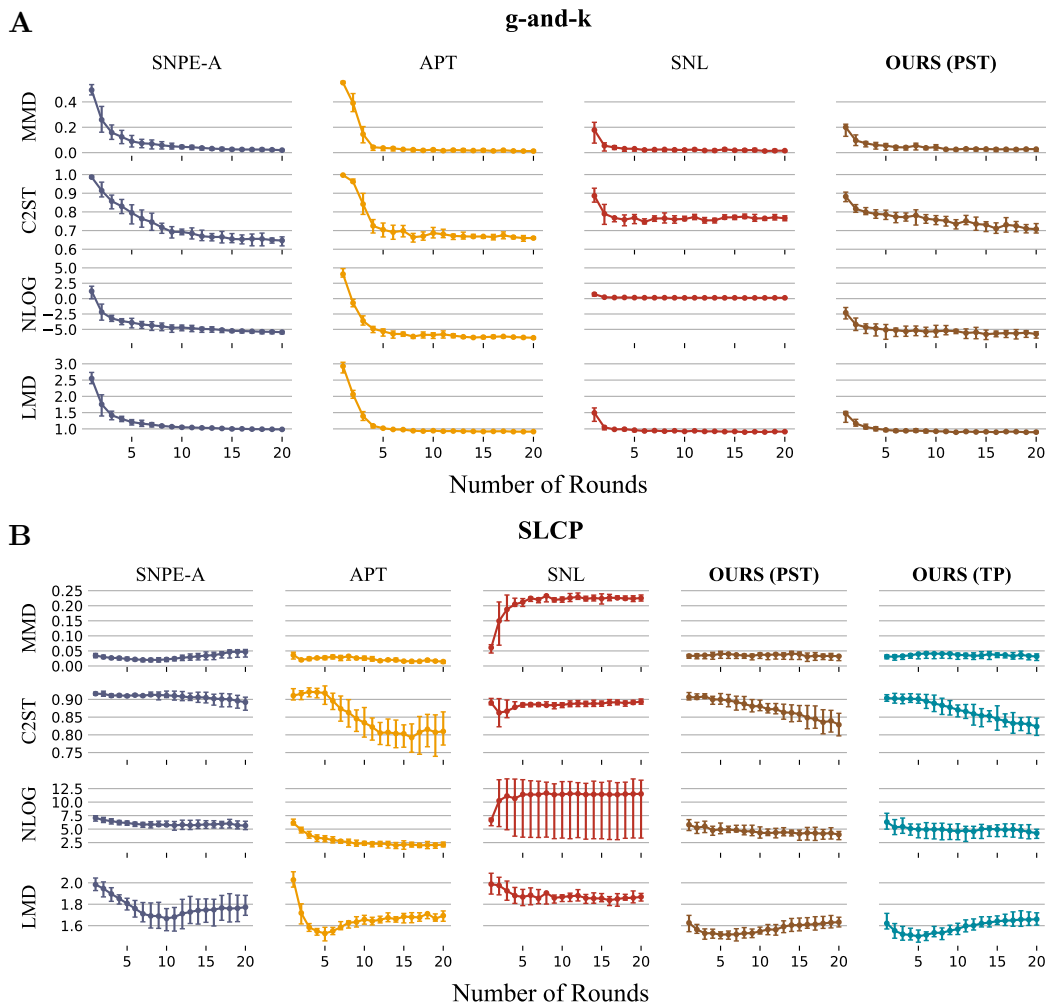


Figure 6: **Our proposed strategy versus other methods.** Due to the unbounded prior for the g-and-k model, we can directly apply the neural posterior and we put the result of this problem in the column of OURS (PST). **A.** Performance on g-and-k model. **B.** Performance on SLCP model. The horizontal axis represents the round of training and the error bars represent the mean with the upper and lower quartiles.

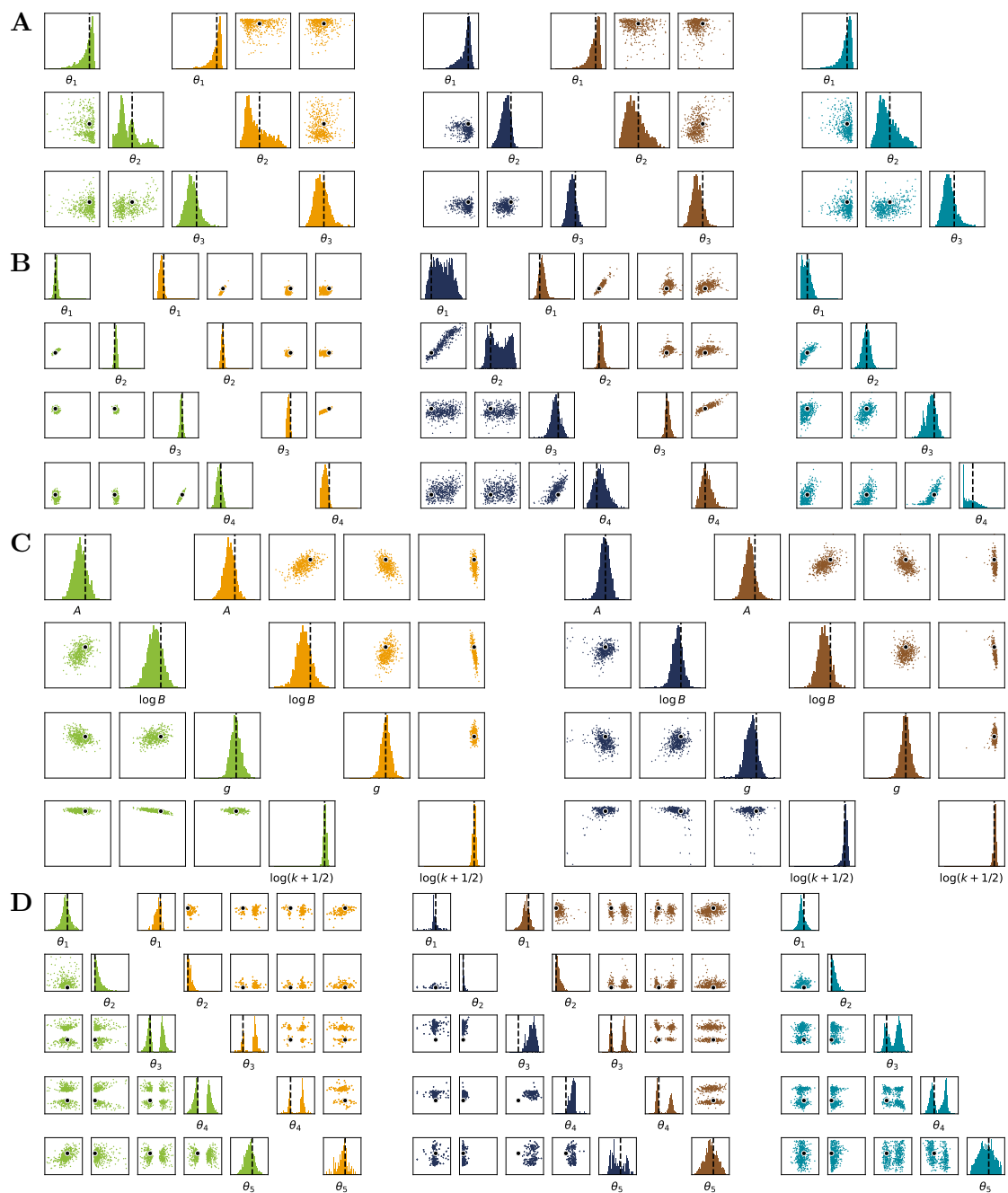


Figure 7: **Comparison of posterior densities evaluating at x_o .** **A.** M/G/1 model. **B.** Lotka-Volterra model. **C.** g-and-k model. **D.** SLCP model. In each set of figures, the near exact ‘True’ posterior obtained by the SMC-ABC method, the APT method, the original SNPE-B method, our proposed method (with PST), and our proposed method (with TP) are presented from left to right. Note that the TP method was not considered for the g-and-k model.